High Definition Diagnostic Imaging: Transversal & Tangential Helix Coupling Control of the Projective Oscillator Representation

Walter Schempp
Lehrstuhl fuer Mathematik I
University of Siegen
57068 Siegen, Germany
schempp@mathematik.uni-siegen.de

In the field of modern radiological diagnostics, the high definition or high contrast–resolution imaging modalities mainly consist of

- Multidetector or Multislice Computed Tomography (MDCT),

and the imaging variant of nuclear magnetic resonance (NMR),

- Non–Invasive Magnetic Resonance Tomography (MRT).

Although MDCT and MRT are in complementary Legendre *duality* in the way the cross–sectional images are generated, there are some striking analogies in the historical development of both clinical imaging modalities. In addition, both high definition imaging procedures are closely related to the projective *oscillator representation* in the context of harmonic analysis on the three–dimensional real Heisenberg unipotent Lie group, and the symplectic group $\mathbf{SL}(2,\mathbb{R})$ canonically embedded into its automorphism group. In the framework of MDCT examinations, the projective oscillator representation gives rise to the standard filtered backprojection image reconstruction algorithm.

As a closed subgroup of $\mathbf{SL}(3,\mathbb{R})$, the three–dimensional real Heisenberg unipotent Lie group forms a *central* extension of the symplectic plane $(\mathbb{R}^2, \det)$ by the real line $\mathbb{R}$ ([27]). The associated three–dimensional real Heisenberg nilpotent Lie algebra is generated by the smooth vector fields

$$X_1 = \frac{\partial}{\partial x} - \frac{1}{2} y \frac{\partial}{\partial z}, \qquad X_2 = \frac{\partial}{\partial y} + \frac{1}{2} x \frac{\partial}{\partial z}, \qquad X_3 = \frac{\partial}{\partial z},$$

and characterized by the Heisenberg commutation relations

$$[X_1, X_3] = [X_2, X_3] = 0\,, \qquad [X_1, X_2] = X_3\,.$$

According to the Stone–von Neumann theorem, there is only *one* equivalence class of irreducible unitary linear representations of the Heisenberg unipotent Lie group with

given central character. Although a representation of this kind is unique up to equivalence, it has many different *concrete* realizations which can be organized into smooth families. This circumstance seems to be at the heart of the transversal and tangential helix coupling control of the oscillator representation which acts as a projective *intertwiner* on the self–adjoint symplectic group $\mathbf{SL}(2,\mathbb{R})$.

The infinitesimal or incremental rotation is represented by the planar rotation of phase angle $\varphi = \frac{\pi}{2}$:

$$\frac{\mathrm{d}}{\mathrm{d}t}\,|_{t=0} \begin{pmatrix} \cos t & -\sin t \\ \sin t & \cos t \end{pmatrix} = \begin{pmatrix} 0 & -1 \\ 1 & 0 \end{pmatrix} = \begin{pmatrix} \cos\frac{\pi}{2} & -\sin\frac{\pi}{2} \\ \sin\frac{\pi}{2} & \cos\frac{\pi}{2} \end{pmatrix} = J\,,$$

where $J^2 = -\mathrm{id}_{\mathbb{R}^2}$ and $J^4 = \mathrm{id}_{\mathbb{R}^2}$. Because the projective oscillator representation assigns to the standard symplectic matrix or Weyl element

$$J = \begin{pmatrix} 0 & -1 \\ 1 & 0 \end{pmatrix} \in \mathbf{SO}(2,\mathbb{R}) \subset \mathbf{SL}(2,\mathbb{R})$$

the one–dimensional Fourier transform along the real line $\mathbb{R}$, the *circular* strategy based on the self–adjoint *maximal* compact subgroup $\mathbf{SO}(2,\mathbb{R})$ of the symplectic group $\mathbf{SL}(2,\mathbb{R})$ is particularly suitable for the implementation via *synchronization* of the standard reconstruction algorithms of CT images. Indeed, the fundamental *Fourier slice theorem* establishes the connection between the Fourier transform and the Radon transform by realizing that the two–dimensional Fourier transform identifies with the one–dimensional Fourier transform along the *radial* direction of the Radon transform ([5]).

The standard filtered backprojection image reconstruction is implemented by the *transpose* of the Radon transform. Due to the Fourier slice theorem, the projective oscillator representation gives rise to the *reproducing kernel* of the transpose of the Radon transform in terms of the one–dimensional Fourier transform and the Maslov index of the metaplectic group ([24], [25]). Based on the application of the Fourier slice theorem, the projective oscillator representation supports the filtered backprojection image reconstruction from volumetric data. The prerequisite for the success of helical CT scanning was the development of slip–ring data–transmission gantries, which eliminated the need to rewind the gantry after each rotation and allowed for continuous data acquisition during multiple rotations. For the first time, volumetric data could be acquired without the danger of misregistration or double registration. The ability to acquire volumetric data paved the way for the development of three–dimensional image *postprocessing* strategies, such as multi–planar reformations (MPRs), maximum intensity projections (MIPs), surface–shaded displays (SSDs), and volume–rendering techniqes (VRTs) to make the initial axial images more useful for the observer by extracting clinically relevant information from the enormous amount of data of more than 300–800 axial images that are generated by an acquisition from a single cardiothoracic MDCT examination.

MIPs are created when a specific projection of view is selected and then rays are cast perpendicularly to the view through the volumetric data, with the maximum value encountered by each ray encoded on a two–dimensional output image. VRTs are the most

complex rendering strategies that allow for the integration of all available information from a volumetric data set with control of the opacity or translucency of selected tissue types. Soft convolution kernels are smoothing the X–ray attenuation profile in the output image and reduce the amount of noise but increase partial voluming. Sharper convolution kernels enhance the interface between structures, which improves edge definition and spatial resolution, but also increases the image noise. Finally, harder kernels are able to improve the diagnostic image interpretability ([6]).

The CT imaging modality was introduced into clinical routine in the early 1970s. Its improvements in terms of innovative technology, clinical applications and performance have revolutionized not only diagnostic radiology, but also the the entire practice of medicine. In the early 1990s, the introduction of *helical* CT replaced the time consuming stop–and–shoot scanning mode of the original single–slice CT modality. Helical scanning is presently the method of choice for the vast majority of multislice CT examinations. It formed a further major step in the development and ongoing technological refinement of the CT imaging modality such as CT angiography ([6], [9], [12], [13], [14], [15], [17]). With helical CT, the patient table is continuously translated along the axial direction while scan data are acquired by the X–ray tube–detector system mounted by means of a *rigidly* coupling yoke on the rotating gantry. To improve the workflow, continuous table move (CTM) is now available also in whole–body MRT. Scanning with CTM is a very new and exciting technology for all applications that require large anatomical coverage, beyond the MRT scanner's intrinsic field–of–view. With the CTM mode, morphological scans are always performed exactly at the isocenter, that is in the region of maximum magnetic field homogeneity. This directly translates into improved image interpretability and diagnostic quality.

Advanced MDCT scanners employ a planar rotate/rotate geometry, in which both the X–ray *photons* emitting tube and the detector bank are rotating simultaneously about the patient. The rigid rotate/rotate motion permits a coupling of the projective oscillator representation to the three–dimensional roto–translation group under its sub–Riemannian geometry of mathematical control theory ([10]) and robotic geometric control theory ([26]): The harmonic oscillator of *bosonic* quantum field theory is approximated by the mathematical pendulum. This three–dimensional real Lie group is the semi–direct product $\mathbf{SO}(2,\mathbb{R}) \lhd \mathbb{R}^2 \subset \mathbf{SL}(3,\mathbb{R})$. The X–ray attenuation profile is measured by the individual elements of the detector bank which rotates simultaneously with the X–ray photons emitting tube. All measurement values acquired at the same angular position of the measurement system, that is, at the same phase angle, are called a projection of view. Typically 1000 projections are measured during each 2π rotation. Each detector element consists of a radiation–sensitive solid–state material such as cadmium tungstate, gadolinium–oxide, or gadolinium oxisulfide with appropriate dopings, which converts the X–ray intensity into visible light. The light is then detected by a silicon photodiode. The resulting electrical current is amplified and then converted into a digital signal.

In 2005, a dual source CT system (DSCT), that is a CT system with *two* X–ray photons emitting tubes and two corresponding detector banks, offset by a phase angle of

Phase angle control: High definition MDCT scanner of the newest generation for cone–beam reconstruction

$\varphi = \frac{\pi}{2}$, was introduced. The key benefit of DSCT is improved temporal resolution. High temporal resolution is mandatory for coronary artery anatomy imaging, as they show strong movement during the cardiac cycle and simultaneously require sub–millimeter spatial resolution. A scanner of DSCT type provides temporal resolution of a quarter of the gantry rotation time and therefore allows for the resolution of the extremely complex three–dimensional motion pattern of the beating heart. The technological improvements of CT scanners have been impressive and 64–slice MDCT has largely superseded four- and 16–slice MDCT scanners, while prototype 256- or even 320–slice MDCT scanners have been introduced very recently in order to compete with 7 Tesla MRT scanners of high magnetic field density ([2]).

By definition, *pitch* is the quotient of table feed per rotation divided by the total width of the collimated X–ray beam. The pitch value controlled multislice data spiral is modelled by the Heisenberg helix which forms a geodesic trajectory

$$\gamma_{\Phi,c} : t \mapsto \left(e^{i\Phi} \frac{1 - e^{-ict}}{c}, \frac{1}{2\,c^2}(ct - \sin ct) \right) \qquad (c \neq 0)$$

within the sub–Riemannian geometry of the three–dimensional real Heisenberg unipotent Lie group ([7], [8]). The Carnot–Carathéodory distance *minimizer* $\gamma_{\Phi,c}$ of phase angle $\Phi \in]-\pi, \pi]$ at the origin, *geodesic* curvature $c \neq 0$, and central oscillating *decoherence* factor $t \mapsto -\frac{1}{2\,c^2} \sin ct$ is a vital prerequisite for the data acquisition strategies in order to reduce ionizing radiation exposure ([11]). According to the Darboux theorem, modulo local change of coordinate charts, the standard differential form

$$\eta = \mathrm{d}z - \frac{1}{2}\,(x\,\mathrm{d}y - y\,\mathrm{d}x)$$

is the *only* contact form on a three–dimensional manifold which gives rise to the voxel identity

$$\eta \wedge \mathrm{d}\eta = -\,\mathrm{d}x \wedge \mathrm{d}y \wedge \mathrm{d}z\,.$$

It follows that the angular contact form of the three–dimensional roto–translation Lie group $\mathbf{SO}(2,\mathbb{R}) \lhd \mathbb{R}^2$ given by

$$\eta_0 = \sin\varphi\,\mathrm{d}x - \cos\varphi\,\mathrm{d}y$$

is locally diffeomorphic to η and therefore allows for the *optimal* tangential trajectory fitting to the Heisenberg helix $\gamma_{\Phi,c}$. The multisegmental synchronization of high in–plane resolution is given by the wedge product of differential forms

$$\eta_0 \wedge \mathrm{d}\eta_0 = -\,\mathrm{d}\varphi \wedge \mathrm{d}x \wedge \mathrm{d}y\,.$$

Provided the three–dimensional *state* manifold underlying the rotate/rotate motion of the rigid X–ray–tube–detector system is coordinatized by the triples $(\varphi, x, y) \in \mathbf{SO}(2,\mathbb{R}) \times \mathbb{R}^2$, the action defined by the smooth vector fields

$$Y_1 = \cos\varphi\,\frac{\partial}{\partial x} + \sin\varphi\,\frac{\partial}{\partial y}, \quad Y_2 = \frac{\partial}{\partial\varphi}, \quad Y_3 = \sin\varphi\,\frac{\partial}{\partial x} - \cos\varphi\,\frac{\partial}{\partial y}$$

of commutation relations

$$[Y_1, Y_3] = 0, \qquad [Y_1, Y_2] = Y_3, \qquad [Y_3, Y_2] = -Y_1,$$

allows for the transversal and tangential coupling of double–oblique image planes to the local curvature of the scanning helix on the circular energy cylinder. The resulting images on the Siemens star like multisegmental foliation *leaves* of overlapping transversal planes that are tangentially coupled to the locally minimizing Heisenberg helix $\gamma_{\Phi,c}$ are generated from high definition *cone–beam* reconstruction via longitudinal reformatting. The rotating flat foliations of phase angle φ correspond exactly to the principal $\mathbf{SL}(2,\mathbb{R})$–bundle of polarization planes of the three–dimensional real Heisenberg Lie algebra with one–dimensional center. The procedure is similar to MPR postprocessing of the filtered backprojection algorithm associated to the projective oscillator representation.

Cardiothoracic MDCT examinations are frequently degraded by motion artifacts caused by cardiac pulsation ([9], [18], [19]). Virtually freezing cardiac motion and eliminating motion artifacts in the cone–beam reconstructed images via synchronization and phase–correlation of the multisegmental foliations of double–oblique flat image leaves

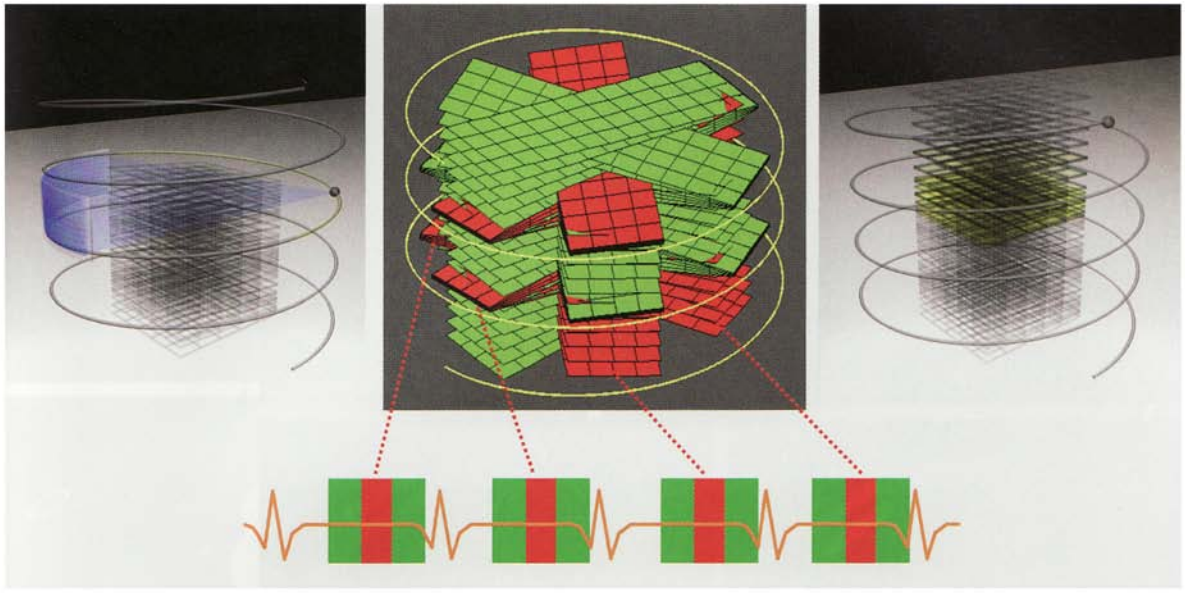

ECG–gated synchronization and phase–correlation for high definition cone–beam image reconstruction

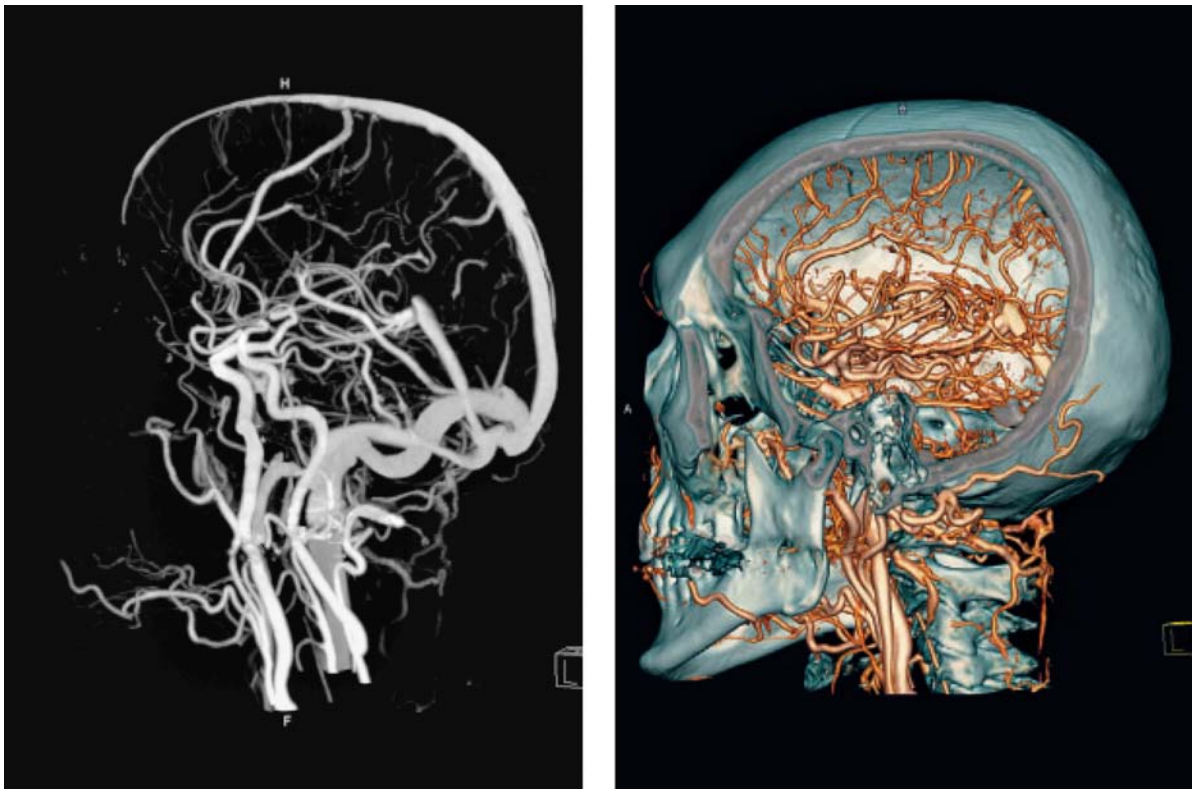

High definition intracranial MDCT–angiography: MIP and VRT postprocessing strategies

in each cardiac cycle with the R peak of the QRS wavelets of the electrocardiogram (ECG) can substantially improve diagnostic image quality ([9]).

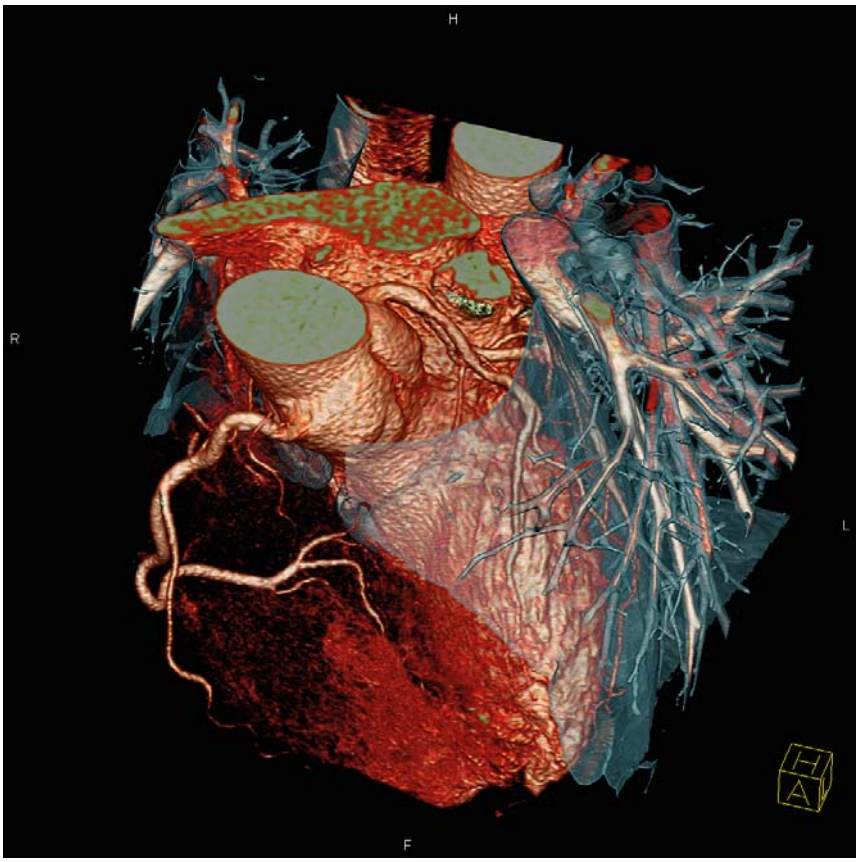

High definition cardiovascular MDCT imaging

Coronary artery imaging is a demanding application for any clinical imaging modality. A highly promising development of the CT modality is cardiovascular imaging with innovative robotic rotating C–arm flat–panel detector based systems. These systems allow for the examination of the complete coronary artery tree within one short breath–hold time to avoid breathing artifacts and to limit the amount of contrast medium administration. Finally, the complementary duality between MDCT and MRT can be seen from the classical isoperimetric inequality

$$\boxed{4\pi F \leq L^2}$$

which *circularly* balances between the maximal magnetic field density F of generating spin coherence by the non–invasive MRT procedure and minimal trajectory length of ionizing radiation exposure in the MDCT modality. Compared with CT angiography, in MRT there is no ionizing radiation and no need for nephrotoxic contrast medium administration. Because pulse squences for MRT angiographic acquisitions are designed so that vascular lumina are the highest intensity structures, MIPs are an efficient strategy to flatten three–dimensional MRT imaging volumes into two–dimensional visualizations ([1], [2], [16], [20]).

Acknowledgments. The author gratefully acknowledges financial support of the European Research Project *Geometrical Analysis in Lie Groups and Applications* (GALA).

MRT Scanner of 3 Tesla magnetic field density and Total Imaging Matrix (TIM) equipment

References

[1] M.A. Bernstein, K.F. King, X.J. Zhou, Handbook of MRI Pulse Sequences. Elsevier Academic Press, Amsterdam, Boston, Heidelberg 2004

[2] D.O. Brunner, N. de Zanche, J. Fröhlich, J. Paska, K.P. Pruessmann, Travelling–wave nuclear magnetic resonance. Nature 457, 994–998 (2009)

[3] M.J. Budoff, S.S. Achenbach, J. Narula, E. Braunwald, Editors, Atlas of Cardiovascular Computed Tomography. Springer–Verlag, Berlin, Heidelberg 2008

[4] C.D. Claussen, E.K. Fishman, B. Marincek, M. Reiser, Editors, Multislice CT: A Practical Guide. Springer–Verlag, Berlin, Heidelberg, New York 2004

[5] S.R. Deans, The Radon Transform and Some of Its Applications. John Wiley & Sons, New York, Chichester, Brisbane 1983

[6] P.J. de Feyter, G.P. Krestin, Editors, Computed Tomography of the Coronary Arteries. Second edition, Informa Healthcare, London 2008

[7] B. Gaveau, Principe de moindre action, propagation de la chaleur et estimées sous–elliptiques sur certains groupes nilpotents. Acta Math. 139, 95–153 (1977)

[8] B. Gaveau, Systèmes dynamiques associés à certains opérateurs elliptiques. Bull. Sc. Math., 2e série, 102, 203–229 (1978)

[9] T.C. Gerber, B. Kantor, E.E. Williamson, Computed Tomography of the Cardiovascular System. Informa Healthcare, London 2007

[10] V. Jurdjevic, Geometric Control Theory. Cambridge University Press, Cambridge, New York, Melbourne 1997

[11] C. Kiefer, Der Quantenkosmos. S. Fischer Verlag, Frankfurt am Main 2008

[12] M. Oudkerk, M.F. Reiser, Coronary Radiology. Second revised edition, Springer–Verlag, Berlin, Heidelberg 2009

[13] G. Pons–Lladó, R. Leta–Petracca, Editors, Atlas of Non–Invasive Coronary Angiography by Mutidetector Computed Tomography. Springer–Verlag, Berlin, Heidelberg 2007

[14] M. Prokop, M. Galanski, Spiral and Multislice Computed Tomography of the Body. Georg Thieme Verlag, Stuttgart, New York 2003

[15] S.V. Raman, P.V. Grodecki, M.J. Garcia, Cardiovascular Multidetector CT Angiography. Informa Healthcare, London 2007

[16] M.F. Reiser, W. Semmler, H. Hricak, Editors, Magnetic Resonance Tomography. Springer–Verlag, Berlin, Heidelberg 2008

[17] M.F. Reiser, C.R. Becker, K. Nikolaou, G. Glazer, Editors, Multislice CT. Third revised edition, Springer–Verlag, Berlin, Heidelberg 2009

[18] M. Rémy–Jardin, J. Rémy, Cardiothoracic Imaging with MDCT. Springer–Verlag, Berlin, Heidelberg 2009

[19] G.D. Rubin, N.M. Rofsky, Editors, CT and MR Angiography: Comprehensive Vascular Assessment. Lippincott Williams & Wilkins. Philadelphia, Baltimore, New York 2009

[20] W.J. Schempp, Magnetic Resonance Imaging: Mathematical Foundations and Applications. Wiley–Liss, New York, Chichester, Weinheim 1998

[21] W. Schempp, Quantum state tomography of nanostructures and the non–linear Heisenberg nilpotent Lie group model of quantum information processing. International Journal of Computing Anticipatory Systems 19, 298–322 (2006)

[22] W.J. Schempp, The Fourier holographic encoding strategy of symplectic spinor visualization. In: New Directions in Holography and Speckle, H.J. Caulfield, Chandra S. Vikram, Editors, pp. 479–522, Amer. Sci. Publishers, Valencia, California 2008

[23] W.J. Schempp, The Legendre duality of CT and MRT diagnostic imaging modalities. Manuscript 2009 (to appear)

[24] L. Schwartz, Sous-espaces hilbertiens d'espaces vectoriels topologiques et noyaux associés (noyaux reproduisants). J. d'Analyse Mathématique, Vol. XIII, 115–256 (1964)

[25] L. Schwartz, Sous-espaces hilbertiens et noyaux associés; applications aux représentations des groupes de Lie. In: Deuxième Colloq. l'Anal. Fonct., pp. 153–163, Centre Belge Recherches Mathématiques, Librairie Universitaire, Louvain 1964

[26] J.M. Selig, Geometrical Methods in Robotics. Springer–Verlag, New York, Berlin, Heidelberg 1996

[27] A. Weil, Sur certains groupes d' opérateurs unitaires. Acta Math. 111, 143–211 (1964); Collected Papers, Vol. III, pp. 1–69, Springer–Verlag, New York, Heidelberg, Berlin 1979